Proceedings Issue: Behavior of Granular Media (2006)

Numerical simulation of powder flow by Finite Element methods

S. Turek and A. Ouazzi
Institute of Applied Mathematics, University of Dortmund, 44227 Dortmund, Germany

Abstract

In contrast to most fluids, flowing powders do not exhibit viscosity such that a Newtonian rheology cannot accurately describe granular flow. Assuming that the material is incompressible, dry, cohesionless, and perfectly rigid-plastic, generalized Navier-Stokes equations ('Schaeffer Model') have been derived where the velocity gradient has been replaced by the shear rate, and the viscosity depends on pressure and shear rate which leads to mathematically complex problems. In this report we present numerical algorithms to approximate these highly nonlinear equations based on finite element methods. First of all, a Newton linearization technique is applied directly to the continuous variational formulation. The approximation of the incompressible velocity field is treated by using stabilized nonconforming Stokes elements and we use a Pressure Schur Complement smoother as defect correction inside of a direct multigrid approach to solve the linear saddle-point problems with high numerical efficiency. The results of computational experiments for two prototypical flow configurations are provided.

1 PHYSICAL BACKGROUND

1.1 Mohr-Coulomb criterion for friction

The Mohr theory suggests that the shear stress on a failure reaches some unique function of normal stress, $\tau = f(\sigma)$, where τ is the shear stress and σ is the normal stress. Coulomb found that for frictional motion the yield shear stress can be expressed as a combination of a normal stress dependent component and a stress independent component. While the normal stress dependent component is connected with the internal angle of friction ϕ, the former seems to be related to the intrinsic cohesion and is denoted by the symbol c. Then, the Coulomb equation reads

$$\tau = \sigma \tan \phi + c, \tag{1}$$

where ϕ and c are the material constants defined as the angle of internal friction and the cohesive strength, respectively; a material is called non-cohesive if $c = 0$. Eq. (1) represents the simple law of friction of two solids sliding on each other with the shear force proportional to the normal force, $\eta = \tan \phi$ being the friction coefficient. A similar condition also exists at the interface between the granular material and the walls of the container: only the angle of internal friction is replaced by the angle of wall friction, ϕ_W. The angle satisfies $\phi_W < \phi$ since the wall is usually less rough than a powder layer; this is mainly due to the void fraction near the wall.

1.2 Regimes of powder flow

Similar to fluid flow, where several characteristic numbers, like Froude number, Reynolds number, etc., can be used to characterize the qualitative flow behavior, the various powder regimes can be represented as a function of a dimensionless shear rate $\gamma^{o*} = \gamma^o [d_p/g]^{1/2}$ which contains a gravitational term g and a particle size d_p (see Tardos et al. [13]). Based on such a characterization, one has the following 3 different regimes.

1.2.1 Quasi-static regime

This regime is valid when the flow is slow enough that any movement between two static states can be neglected; then the static equilibrium equation can be applied. With this approach only stress and condition of the onset of flow can be computed, while no flow field can be predicted which circumscribes the range of applications of this approach. There is a large number of analytical and numerical solutions to this case

and an important number of literature devoted to this regime, see for instance [3], [7].

1.2.2 Slow and frictional regime

In this regime the frictional forces between particles are predominant, so the inertial effect is added to the static equations as well as the consideration of continuity beside a yield condition. The first model invoking a flow rule was introduced by Schaeffer (1987) [10]. This regime is very important since it can be used for modeling a wide range of practical phenomenon and industrial applications. However, for the serious challenges which arise in this regime, for instance ill-posed partial differential equations and the prediction of stress fluctuations, there is still a lack of fundamental research so that dealing with these problems requires a multidisciplinary treatment. Our research has the goal of supporting this part by modern numerical methods which will be described in the subsequent sections.

1.2.3 Intermediate and rapid granular regimes

For the intermediate regime, additional to inter-particle friction energy, collision energy is important, too. For the rapid regime, the short particle-particle contacts are important while frictional forces are neglected. This regime is often described via kinetic models and will not be treated in this paper. It is mentioned here just to have a complete view on the different regimes of powder flow (see [13] for more details).

1.3 Flow rule: Saint Venant principle

The Saint Venant principle of solid mechanics says that stresses cause deformations preferentially in the same direction. This leads to the co-axiality flow rule condition which states that the principal directions of the stress and rate deformation are parallel and neglect the rotation of a material element during deformation. In two-dimensional Cartesian coordinates, this condition takes the form, for example:

$$\frac{\mathbf{T}_{xx} - \mathbf{T}_{yy}}{\mathbf{T}_{xy}} = \frac{2(\partial u/\partial x - \partial v/\partial y)}{\partial u/\partial x + \partial v/\partial y} \qquad (2)$$

This was postulated by Schaeffer [10] for the deformation of granular material. However, since the deformation of the granular material requires that the stresses in different directions must be different, Schaeffer claimed that ***"the response of the material to such unequal stresses should be to contract in the directions of greater stress and to expand in the directions of smaller stress".*** This reflects the requirement that the eigenvectors of stress tensor and strain rate are aligned and it quantitatively links the deviatoric stress and the strain rate tensor by the formula $\mathbf{S} = \lambda \mathbf{D}$.

1.4 Rigid perfect plastic behavior

1.4.1 Plastic deformation

The deformation of a granular material is considered to be plastic in the sense that, if after deformation the shearing stress is reduced, the material would not show any tendency to return to its original state. Plastic deformation was already proposed by E. C. Bingham, in 1922, in the context of non-Newtonian fluids, and in which the rheological behavior is governed by the following equation introduced by Oldroyd in modified state:

$$\mathbf{T} = -pI + (\frac{\mu_0}{\|\mathbf{D}\|} + \mu)\mathbf{D} \qquad (3)$$

1.4.2 Dilatancy

A simple manifestation of this phenomenon occurs when one leaves dry footprints while walking along a wet beach: the deformed sand dilates, therefore space between grains increases, allowing for upper water to invade the sand. As a consequence, footsteps get dry and water goes down. This is the phenomenon of dilatancy which was explained by Reynolds in 1885, and demonstrated experimentally: a glass tube attached to a balloon showed that the amount of excess water decreased when the sand was deformed, thus showing that deformation increases the space between grains. Dilatancy is important in the dynamics of granular material, introducing a stick-slip instability at low velocity (see [6]), and it occurs because each grain needs more space in the flowing state than at rest. Then, the flow theory of plasticity must be applied to the constitutive modeling for describing the deformation process of a granular material.

2 CONSTITUTIVE EQUATIONS FOR POWDER FLOW

2.1 Equation of motion

The powder is assumed to be an incompressible continuum that obeys conservation of mass and momentum (density ρ, gravity $\mathbf{g}$, velocity $\boldsymbol{u}$):
Conservation of mass: With material derivative $\frac{D*}{Dt}$, there holds $\frac{D\rho}{Dt} = \frac{\partial \rho}{\partial t} + \nabla \cdot (\rho \boldsymbol{u}) = 0$.
Incompressible material: The bulk density, ρ, is a constant, so that $\nabla \cdot \boldsymbol{u} = 0$.
Equation of motion: With $\mathsf{T} = \mathsf{S} - p\mathsf{I}$, there holds $\rho \frac{D\boldsymbol{u}}{Dt} = \nabla \cdot \mathsf{T} + \rho \mathbf{g}$.

2.2 Constitutive equations

The constitutive equation is devoted to correlate between the deviatoric tensor S and the velocity, through the second invariant of the rate deformation $D_{II} = \frac{1}{2}\mathsf{D} : \mathsf{D}$, where the rate of deformation is given by $\mathsf{D} = \frac{1}{2}(\nabla \boldsymbol{u} + \nabla^T \boldsymbol{u})$. There are several examples:
Newtonian law: $\mathsf{S} = 2\nu_0 \mathsf{D}$
Power law: $\mathsf{S} = 2\nu(D_{II})\mathsf{D}, \quad \nu(z) = z^{\frac{r}{2}-1}, \quad r \geq 1$ ($r = 1$: **Bingham law**)
Schaeffer's law: For a powder, a constitutive equation was first introduced by Schaeffer [10] which has to obey a

- yield condition: $\|\mathsf{S}\| = \sqrt{2} p \sin\phi$,
- flow rule: $\mathsf{S} = \lambda \mathsf{D} \quad$ with $\lambda \geq 0$.

In fact, the flow rule is based on a yield criterion for granular materials of von Mises type, which is basically derived from a law of sliding friction applied to the individual particles. Specifically in terms of the principal stresses σ_i, this condition is written as

$$\sum_{i=1}^{3} (\sigma_i - p)^2 \leq k^2 p^2 \quad \text{with} \quad p = \frac{1}{3} \operatorname{tr} \mathsf{T} \tag{4}$$

where $k = \sqrt{2}\sin\phi$ is a characteristic constant of the material, and σ_i are the eigenvectors of T_{ij}. For a material that deforms plastically, equality must hold in Eq. (4):

$$\sum_{i=1}^{3} (\sigma_i - p)^2 = k^2 p^2 \tag{5}$$

Under plane strain $p = \frac{1}{2}(\sigma_1 + \sigma_2)$, we may consider a strictly 2D-yield condition:

$$(\sigma_1 - p)^2 + (\sigma_2 - p)^2 = 2p^2 \sin^2\phi \tag{6}$$

A constitutive equation between stress and strain rate was proposed for slow powder by Schaeffer [10]. This equation obeys the von Mises yield condition and the described flow rule:

$$\mathsf{T} = -pI + \sqrt{2} p \sin\phi \frac{\mathsf{D}}{\|\mathsf{D}\|} \text{ if } D \neq 0 \tag{7}$$

In fact, the flow rule is assumed to have the form $\mathsf{T} = -pI + \lambda \mathsf{D}$, where λ is a coefficient. To satisfy the yield condition of the given flow rule in terms of von Mises, i.e. $\|\mathsf{S}\| = \sqrt{2} p \sin\phi$, then there must hold:

$$\lambda = \frac{\sqrt{2} p \sin\phi}{\|\mathsf{D}\|} \tag{8}$$

We use this correlation to obtain finally the constitutive equation $\mathsf{T} = -pI + \sqrt{2} p \sin\phi \frac{\mathsf{D}}{\epsilon + \|\mathsf{D}\|}$, where ϵ is a typical (small) regularization parameter.

2.3 Generalized flow equations

The problem can be stated in the framework of the generalized incompressible Navier-Stokes equations:

$$\rho \frac{Du}{Dt} = -\nabla p + \nabla \cdot (\nu(p, D_{II})\mathsf{D}) + \rho g, \quad \nabla \cdot \boldsymbol{u} = 0$$

If we define the nonlinear pseudo viscosity $\nu(\cdot,\cdot)$ as a function of the second invariant of the rate deformation D_{II} and the 'pressure' p, we can show that different materials can be ranged within different viscosity laws including powder;

- Power law defined for $\nu(z,p) = \nu_0 z^{\frac{r}{2}-1}$
- Bingham law defined for $\nu(z,p) = \nu_0 z^{-\frac{1}{2}}$
- Schaeffer's law (including the 'pressure') defined for $\nu(z,p) = \sqrt{2}\sin\phi\, p z^{-\frac{1}{2}}$

3 Problem formulation

Let us consider the flow of the stationary generalized Navier-Stokes problem in (2.3) in a bounded domain $\Omega \subset \mathbb{R}^2$. If we restrict the set V of test functions to be divergence-free and if we take the constitutive laws into account, the above equations from (2.3) lead to:

$$\int_\Omega 2\nu(D_{II}(\boldsymbol{u}), p)\mathsf{D}(\boldsymbol{u}) : \mathsf{D}(\boldsymbol{v})\, dx + \int_\Omega (\boldsymbol{u} \cdot \nabla \boldsymbol{u})\boldsymbol{v}\, dx = \int_\Omega \boldsymbol{f}\boldsymbol{v}\, dx, \qquad \forall \boldsymbol{v} \in V \tag{9}$$

It is straightforward to penalize the constraint $\operatorname{div} \boldsymbol{v} = 0$ to derive the equivalent mixed formulations of (9): Find $(\boldsymbol{u}, p) \in X \times M$ (with the spaces $X = H_0^1(\Omega)$ and $M = L^2(\Omega)$) such that:

$$\int_\Omega 2\nu(D_{II}(\boldsymbol{u}), p)\mathbf{D}(\boldsymbol{u}) : \mathbf{D}(\boldsymbol{v})\, dx + \int_\Omega (\boldsymbol{u} \cdot \nabla \boldsymbol{u}) v\, dx$$

$$+ \int_\Omega p \operatorname{div} \boldsymbol{v}\, dx = \int_\Omega \boldsymbol{f}\boldsymbol{v}\, dx, \qquad \forall \boldsymbol{v} \in X,$$

$$\int_\Omega q \operatorname{div} \boldsymbol{u}\, dx = 0, \qquad \forall q \in M \tag{10}$$

3.1 Nonlinear solver: Newton iteration

In this approach, the nonlinearity is first handled on the continuous level. Let $\boldsymbol{u}^l$ being the initial state, the (continuous) Newton method consists of finding $\boldsymbol{u} \in V$ such that

$$\int_\Omega 2\nu(D_{II}(\boldsymbol{u}^l), p^l)\mathbf{D}(\boldsymbol{u}) : \mathbf{D}(\boldsymbol{v}) dx$$

$$+ \int_\Omega 2\partial_1\nu(D_{II}(\boldsymbol{u}^l), p^l)[\mathbf{D}(\boldsymbol{u}^l) : \mathbf{D}(\boldsymbol{u})][\mathbf{D}(\boldsymbol{u}^l) : \mathbf{D}(\boldsymbol{v})] dx$$

$$+ \boxed{\int_\Omega 2\partial_2\nu(D_{II}(\boldsymbol{u}^l), p^l)[\mathbf{D}(\boldsymbol{u}^l) : \mathbf{D}(\boldsymbol{v})] p dx} = \int_\Omega \boldsymbol{f}\boldsymbol{v}$$

$$- \int_\Omega 2\nu(D_{II}(\boldsymbol{u}^l), p^l)\mathbf{D}(\boldsymbol{u}^l) : \mathbf{D}(\boldsymbol{v}) dx, \quad \forall \boldsymbol{v} \in V\,, \tag{11}$$

where $\partial_i\nu(\cdot,\cdot); i = 1, 2$ is the partial derivative of ν related to the first and second variables, respectively. To see this, set $\boldsymbol{X} = \mathbf{D}(\boldsymbol{u}^l), \boldsymbol{x} = \mathbf{D}(\boldsymbol{u}), Y = p^l, y = p, F(\boldsymbol{x}, y) = \nu(\frac{1}{2}|\boldsymbol{x}|^2, y)\boldsymbol{x}$ and $f(t) = F(\boldsymbol{X}+t\boldsymbol{x}, Y+ty)$, so that

$$\begin{aligned} \partial_{x_j} F_i(\boldsymbol{x}, y) &= \partial_{x_j}\nu(\tfrac{1}{2}|\boldsymbol{x}|^2, y)x_j x_i + \nu(\tfrac{1}{2}|\boldsymbol{x}|^2, y)\delta_{ij} \\ \partial_y F_i(\boldsymbol{x}, y) &= \partial_y\nu(\tfrac{1}{2}|\boldsymbol{x}|^2, y)x_i \end{aligned} \tag{12}$$

where δ_{ij} stands for the standard Kronecker symbol. Having

$$\begin{aligned} f_i'(t) &= \textstyle\sum_j \partial_{x_j} F_i(\boldsymbol{X} + t\boldsymbol{x}, Y + ty)x_j \\ &\quad +\partial_y F_i(\boldsymbol{X} + t\boldsymbol{x}, Y + ty)y \\ &= \nu(\tfrac{1}{2}|\boldsymbol{X} + t\boldsymbol{x}|^2, Y + ty)\boldsymbol{x}_i \\ &\quad +\partial_1\nu(\tfrac{1}{2}|\boldsymbol{X} + t\boldsymbol{x}|^2, Y + ty) \\ &\quad \langle \boldsymbol{X} + t\boldsymbol{x}, \boldsymbol{x}\rangle(\boldsymbol{X}_i + t\boldsymbol{x}_i) \\ &\quad +\partial_2\nu(\tfrac{1}{2}|\boldsymbol{X} + t\boldsymbol{x}|^2, Y + ty)y(\boldsymbol{X}_i + t\boldsymbol{x}_i) \end{aligned} \tag{13}$$

we decrease t towards zero, such that we obtain the Frechet derivative:

$$\begin{aligned} \nabla \cdot[& \ 2\nu(D_{II}(\boldsymbol{u}^l), p^l)\mathbf{D}(\boldsymbol{u}) \\ + & \ 2\partial_1\nu(D_{II}(\boldsymbol{u}^l), p^l)(\mathbf{D}(\boldsymbol{u}^l) : \mathbf{D}(\boldsymbol{u}))\mathbf{D}(\boldsymbol{u}^l) \\ + & \ 2\partial_2\nu(D_{II}(\boldsymbol{u}^l), p^l)p\mathbf{D}(\boldsymbol{u}^l)] \end{aligned} \tag{14}$$

3.2 New linear auxiliary problem

The resulting auxiliary subproblems in each Newton step consist of finding $(\boldsymbol{u}, p) \in X \times M$ as solutions of the linear (discretetized) systems

$$\begin{cases} A(\boldsymbol{u}^l, p^l)\boldsymbol{u} + \delta_d A^*(\boldsymbol{u}^l, p^l)\boldsymbol{u} + Bp & +\delta_p B^*(\boldsymbol{u}^l, p^l)p \\ & = R_u(\boldsymbol{u}^l, p^l), \\ B^T\boldsymbol{u} & = R_p(\boldsymbol{u}^l, p^l), \end{cases} \tag{15}$$

where $R_u(\cdot,\cdot)$ and $R_p(\cdot,\cdot)$ denote the corresponding nonlinear residual terms for the momentum and continuity equations, and the operators $A(\boldsymbol{u}^l, p^l), B, A^*(\boldsymbol{u}^l, p^l)$ and $B^*(\boldsymbol{u}^l, p^l)$ are defined as follows:

$$\langle A(\boldsymbol{u}^l, p^l)\boldsymbol{u}, \boldsymbol{v}\rangle = \int_\Omega 2\nu(D_{II}(\boldsymbol{u}^l), p^l)\mathbf{D}(\boldsymbol{u}) : \mathbf{D}(\boldsymbol{v})\, dx \tag{16}$$

$$\langle Bp, \boldsymbol{v}\rangle = \int_\Omega p\nabla \cdot \boldsymbol{v}\, dx \tag{17}$$

$$\langle A^*(\boldsymbol{u}^l, p^l)\boldsymbol{u}, \boldsymbol{v}\rangle = \int_\Omega 2\partial_1\nu(D_{II}(\boldsymbol{u}^l), p^l)[D(\boldsymbol{u}^l) : D(\boldsymbol{u})][D(\boldsymbol{u}^l) : D(\boldsymbol{v})]\, dx \tag{18}$$

$$\langle B^*(\boldsymbol{u}^l, p^l)\boldsymbol{v}, p\rangle = \int_\Omega 2\partial_2\nu(D_{II}(\boldsymbol{u}^l), p^l)[D(\boldsymbol{u}^l) : D(\boldsymbol{v})]p\, dx \tag{19}$$

4 Discretization

We consider a subdivision $T \in \mathcal{T}_h$ consisting of quadrilaterals in the domain $\Omega_h \in \mathbb{R}^2$, and we employ rotated bilinear nonconforming elements [9]. For any quadrilateral T, let (ξ, η) denote a local coordinate system obtained by joining the midpoints of the opposing faces of T. Then, in the *nonparametric* case, we set on each element T

$$\tilde{Q}_1(T) := span\left\{1, \xi, \eta, \xi^2 - \eta^2\right\}. \tag{20}$$

The degrees of freedom are determined by the nodal functionals $\{F_\Gamma^{(a,b)}(\cdot), \Gamma \subset \partial\mathcal{T}_h\}$,

$$F_\Gamma^a := |\Gamma|^{-1} \int_\Gamma v d\gamma \quad \text{or} \quad F_\Gamma^b := v(m_\Gamma) \tag{21}$$

$$(m_\Gamma \text{ midpoint of edge } \Gamma)$$

such that the finite element space can be written as

$$W_h^{a,b} := \left\{ \begin{array}{l} v \in L_2(\Omega_h), v \in \tilde{Q}_1(T), \forall T \in \mathcal{T}_h, \\ v \text{ continuous w.r.t. all nodal functionals} \\ F_{\Gamma_{i,j}}^{a,b}(\cdot), \text{ and } F_{\Gamma_{i0}}^{a,b}(v) = 0, \forall \Gamma_{i0} \end{array} \right\}. \tag{22}$$

Here, $\Gamma_{i,j}$ denote all inner edges sharing the two elements i and j, while Γ_{i0} denote the boundary edges of $\partial\Omega_h$. In this paper, we always employ version 'a' with the integral mean values as degrees of freedom. Then, the corresponding discrete functions will be approximated in the spaces

$$\begin{aligned} V_h &:= W_h^{a,b} \times W_h^{a,b} \\ L_h &:= \left\{q_h \in L^2(\Omega), q_{h|T} = \text{const.}, \forall \mathcal{T} \in \mathcal{T}_h\right\}. \end{aligned} \tag{23}$$

Due to the nonconformity of the discrete velocities, the classical discrete 'Korn's Inequality' is not satisfied which is important for problems involving the symmetric part of the gradient [5]. Therefore, appropriate edge-oriented stabilization techniques (see [2, 4, 15, 8] have to be included which directly treat the jump across the inter-elementary boundaries via adding the following bilinear form

$$\sum_{edges E} \frac{1}{|E|} \int_E [\phi_i][\phi_j] d\sigma \tag{24}$$

for all basis functions ϕ_i and ϕ_j of $W_h^{a,b}$. Taking into account an additional relaxation parameter $s = s(\nu)$, the corresponding stiffness matrices are defined via:

$$\langle S\boldsymbol{u}, \boldsymbol{v}\rangle = s \sum_{E \in E_I \cup E_D} \frac{1}{|E|} \int_E [\boldsymbol{u}][\boldsymbol{v}] d\sigma \tag{25}$$

Here, the jump of a function $\boldsymbol{u}$ on an edge E is given by

$$[\boldsymbol{u}] = \begin{cases} \boldsymbol{u}^+ \cdot \boldsymbol{n}^+ + \boldsymbol{u}^- \cdot \boldsymbol{n}^- & \text{on } E_I, \\ \boldsymbol{u} \cdot \boldsymbol{n} & \text{on } E_D, \\ 0 & \text{on } E_N, \end{cases} \tag{26}$$

where E_I, E_D and E_N are the internal, Dirichlet boundary and Neumann boundary edges respectively and $\boldsymbol{n}$ is the outward normal to the edge and $(\cdot)^+$ and $(\cdot)^-$ indicate the value of the generic quantity $(\cdot)$ on the two elements sharing the same edge.

5 Linear solver

This section is devoted to give a brief description of the involved solution techniques for the resulting linear systems. For the nonconforming Stokes element $\tilde{Q}_1/Q_0$, a 'local pressure Schur complement' preconditioner (see [14]) as generalization of so-called 'Vanka smoothers' is constructed on patches Ω_i which are ensembles of one single or several mesh cells, and this local preconditioner is embedded as global smoother into an outer block Jacobi/Gauss-Seidel iteration which acts directly on the coupled systems of generalized Stokes, resp., Oseen type as described in [15]. If we denote by $\tilde{R}_u$ and $\tilde{R}_p$ the discrete residuals for the momentum and continuity equation which include the complete stabilisation term due to the modified bilinear form S as described in (25), one smoothing step in defect-correction notation can be described as

$$\begin{bmatrix} \boldsymbol{u}^{l+1} \\ p^{l+1} \end{bmatrix} = \begin{bmatrix} \boldsymbol{u}^{l} \\ p^{l} \end{bmatrix} + \omega^l \sum_i \begin{pmatrix} F + S_{|\Omega_i} & \tilde{B} + \delta_p \tilde{B}^*_{|\Omega_i} \\ \tilde{B}^T_{|\Omega_i} & 0 \end{pmatrix}^{-1} \begin{bmatrix} \tilde{R}_u(\boldsymbol{u}^l, p^l) \\ \tilde{R}_p(\boldsymbol{u}^l, p^l) \end{bmatrix} \tag{27}$$

with matrix $F = \tilde{A} + \delta_d \tilde{A}^*$ and $\tilde{A}, \tilde{B}, \tilde{A}^*$ and $\tilde{B}^*$ are the discrete matrices corresponding to the operators in (16), (17), (18) and (19). All other components in the multigrid approach, that means intergrid transfer, coarse grid correction and coarse grid solver, are the

standard ones and are based on the underlying hierarchical mesh hierarchy and the properties of the nonconforming finite elements (see [14] and [15] for the details).

6 NUMERICAL SIMULATIONS

The purpose of this section is to show that our numerical approaches based on FEM techniques are well suited to address the illustrated type of nonlinear powder problems and lead to comparative results with related experiments. Therefore, we consider the following two configurations, powder flow in a Couette device with an obstacle and granular flow in a hopper.

6.1 Drag force in powder flow

As we described before, granular materials can flow like fluids and resist the motion of objects moving through them. Since this retarding force, known as drag force $F_d = (\oint_{C_0} \mathbf{T}\boldsymbol{n}\, ds)_y$ with $(.)_y$ denoting the y-component, see Fig. 1, can be easily measured experimentally for a granular medium in a Couette device with an immersed cylinder [1], for this reason we choose this configuration for our computation: Although our simulation is only in 2D, a lot of characteristics of granular flow can be examined numerically such that at least qualitative comparisons can be obtained.

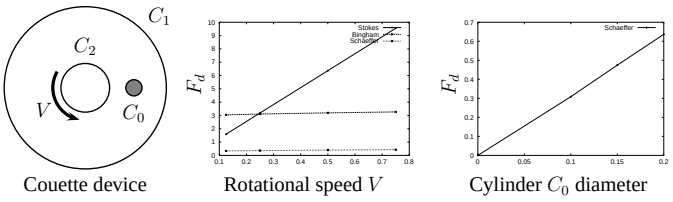

Figure 1: Drag force F_d versus rotational speed V of the cylinder walls in a Couette device ('flow around a cylinder') for different material laws and for varying cylinder diameter. The inner cylinder C_2 is rotating with rotational speed V while the outer cylinder C_1 and the inner cylinder C_0 are fixed; all quantities are in non-dimensional form and shall provide qualitative comparisons only.

As expected, the drag force F_d for Schaeffer and Bingham flow acting on the cylinder C_0 is independent of the velocity, contrary to the (newtonian) Stokes flow, while the drag force increases with larger diameters for the interior cylinder C_0.
In Table 1, we show this behavior more in detail: Here, we perform tests for various prescribed mean pressure values to obtain a unique solution, and for several rotational speeds. As explained before, the Stokes and Bingham model lead to drag forces which are independent of the given mean pressure while the Schaeffer model shows the expected dependence since the pressure is part of the viscous term.
Moreover, we also examine the influence of neglecting the convective terms in the Schaeffer model, that means $(\boldsymbol{u} \cdot \nabla \boldsymbol{u})$ in (9) which is typically done due to the assumption of "slow" flow. Here, we increase continuously the rotational speed V of the inner cylinder C_2 and plot in Figure 2 the behavior of the resulting drag force F_d for the Schaeffer model with and without convection. As can be seen, if we totally neglect the convective term, then the drag force remains constant with an absolute value which is independent of the prescribed velocity. In addition, at least for 'slow' flow, there is no difference between the Stokes and the full Navier-Stokes model, including the convective terms, while from a certain speed on, differences between both models get visible. So, it might be interesting for future experiments to check whether this calculated relation between drag force and increasing velocity can be actually observed, which is at least questionable since the Schaeffer model has been theoretically derived for 'slow' (?) flow only. However, from a numerical point of view, it is reasonable to include this convective part, too, in corresponding numerical modeling and simulation.

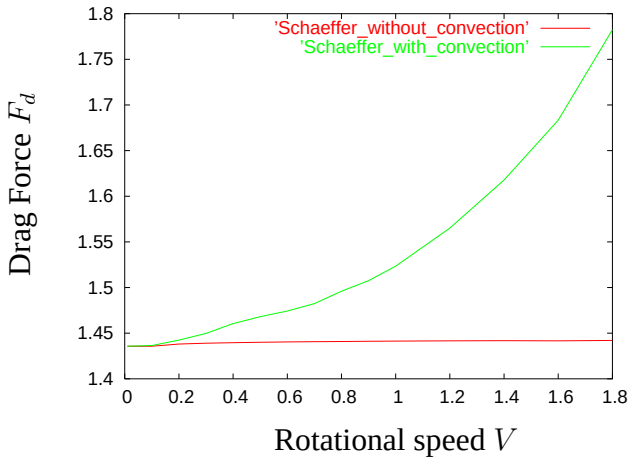

Figure 2: Dependence of the drag force F_d from the rotational speed V for the Schaeffer model with and without convective term

pressure	0.5	1	5	10	100
Speed			Stokes law without convection		
0.05	0.62877D+01	0.62877D+01	0.62877D+01	0.62877D+01	0.62877D+01
0.1	0.12575D+02	0.12575D+02	0.12575D+02	0.12575D+02	0.12575D+02
0.2	0.25151D+02	0.25151D+02	0.25151D+02	0.25151D+02	0.25151D+02
0.5	0.62877D+02	0.62877D+02	0.62877D+02	0.62877D+02	0.62877D+02
Speed			Bingham law without convection		
0.05	0.38137D+01	0.38137D+01	0.38137D+01	0.38137D+01	0.38137D+01
0.1	0.38222D+01	0.38222D+01	0.38222D+01	0.38222D+01	0.38222D+01
0.2	0.38252D+01	0.38252D+01	0.38252D+01	0.38252D+01	0.38252D+01
0.5	0.38265D+01	0.38265D+01	0.38265D+01	0.38265D+01	0.38265D+01
Speed			Schaeffer law without convection		
0.05	0.50419D+00	0.10084D+01	0.50419D+01	0.10084D+02	0.10084D+03
0.1	0.50629D+00	0.10126D+01	0.50628D+01	0.10126D+02	0.10126D+03
0.2	0.50756D+00	0.10151D+01	0.50755D+01	0.10151D+02	0.10151D+03
0.5	0.50849D+00	0.10170D+01	0.50849D+01	0.10170D+02	0.10170D+03

Table 1: The dependence of the drag force from various rotational speed V at different mean pressure values

6.2 Granular flow in a hopper

Flow of granular material in hoppers under gravity is quite complex and experimental approaches show limitations in understanding some phenomena for this type of geometry. Our current investigation is to understand some typical phenomena related to granular material, namely oscillating phenomena and instabilities, as for instance shear banding instabilities.

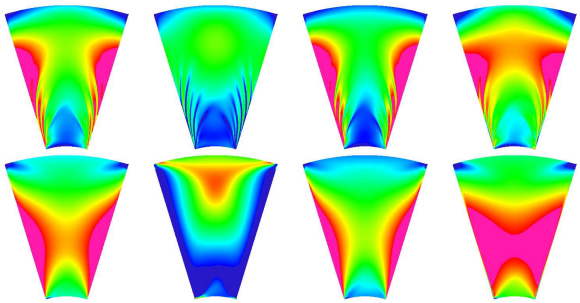

Figure 3: The plot of the pressure, the pseudo viscosity (see (2.3)) and the components σ_{11}, σ_{22} of the stress at t=0.03s for Schaeffer (top) and Bingham law (bottom)

For the Schaeffer model, Figure 3 shows that the flow is significantly influenced by the pressure in the material law, in contrast to the Bingham model which is independent of it. To go deeper in understanding the instability phenomena we plot for different times the average stress for both models in Figure 4. These instabilities may be explained by the stability analysis of Schaeffer [11] who shows the previously illustrated ill-posedness of the problem. However, since we observe that these instabilities arise from the artificial inflow/outflow regions, the influence of the applied boundary conditions is not clear yet. Since the inflow and outflow boundary condition supplied to the hopper do not have any physical meaning, they could be the source of the appearance of the oscillations, too. So, in future, we will examine a new silo geometry with a much longer bin on the bottom and the top of the hopper to diminish the influence of the boundary conditions onto the flow behavior in the constriction.

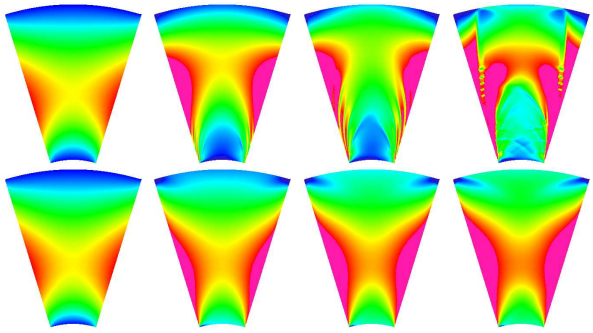

Figure 4: Snapshots of the average stress at t=0.0s, 0.012s, 0.03s and 0.06s for Schaeffer (top) and Bingham law (bottom)

7 Conclusions

Our conclusion is that finite element methods together with special material laws can be useful tools for the numerical simulation of incompressible granular powder, since the complete structure of the flow is involved, i.e. the velocity, the pressure as well as the stress. Although our computer simulation is only two-dimensional it can confirm well known physical behavior, namely the independence of the drag force from the velocity grain and the propagation of a pressure wave in the hopper which may lead to a shear banding instability. At first glance, the shear banding phenomenon gives the impression to be treated mathematically as a discontinuity, but this would cause severe problems for numerical algorithms. On the other hand, shear bands might not be a true physical discontinuity, rather than a change in the involved physical system which could be captured with a compressible model.

Furthermore, the proposed incompressible model for granular and powder flow presents some other disadvantages, like for instance the wrong prediction of the flow rate through a symmetric silo by more than a factor of 4 in comparison with experiments [12]. This gives another motivation to proceed toward compressible granular materials which can be specified via the yield condition $q(p, \rho)$ given in Table 2 (see the work by Tardos and particularly [13] for the details). Then, the flow can be described by a generalized compressible Navier-Stokes-like equation (28) where a mass conservation equation (29) must hold. However, this is not enough because the density ρ is now a depen-

Powder properties	Non-cohesive	Cohesive
Incompressible	$p\sin\phi$	$p\sin\phi + c\cos\phi$
Compressible	$p\sin\phi\left[2-\frac{p}{\rho^{\frac{1}{\beta}}}\right]$	$p\sin\phi\rho^{\frac{1}{\beta}} - C\frac{(p-\rho^{\frac{1}{\beta}})^2}{\rho^{\frac{1}{\beta}}}$

Table 2: Yield condition $q(p,\rho)$ for incompressible and compressible powder ($0.001 < \beta < 0.01$)

dent variable, rather than a constant:

$$\rho\frac{D\boldsymbol{u}}{Dt} = \nabla\cdot\left[\frac{q(p,\rho)}{\left\|\mathbf{D}-\frac{1}{n}\nabla\cdot\boldsymbol{u}\mathbf{I}\right\|}\left(\mathbf{D}-\frac{1}{n}\nabla\cdot\boldsymbol{u}\mathbf{I}\right)\right] - \nabla p + \rho g \qquad n=2,3 \tag{28}$$

$$\frac{\partial\rho}{\partial t} + \nabla\cdot(\rho\boldsymbol{u}) = 0 \tag{29}$$

In order to complete the system, an additional equation is required in the form of the so-called normality condition:

$$\nabla\cdot\boldsymbol{u} = \frac{\partial q(p,\rho)}{\partial p}\left\|\mathbf{D}-\frac{1}{n}\nabla\cdot\boldsymbol{u}\mathbf{I}\right\| \tag{30}$$

Since the presented mathematical and computational methodology in this paper can be naturally extended to these compressible granular and powder flow models, our next step is to present the corresponding results and comparisons in forthcoming papers.

References

[1] Albert, A., Pfeifer, M. A., Brabasi, A. L., and Schiffer, P. Slow drag in granular medium. *Phys. Rev. Lett*, 82:205–208, 1999.

[2] Brenner, C. S. Korn's Inequalities for Piecewise H^1 Vector Fields. *Math. Comp.*, 73:1067–1087, 2004.

[3] Gremaud, P. and Matthews, J. V. On the Computation of Steady Hopper Flows: I, Stress Determination for Coulomb Materials. Technical report, NCSU-CRSC Tech Report CRSC-TR99-35, 2001.

[4] Hansbo, P. and Larson, M. G. A Simple Nonconforming Bilinear Element for the Elasticity Problem. Preprint 2001-01, Chalmers Finite Element Center, Chalmers University of Technology, Göteborg Sweden, 2001.

[5] Knobloch, P. On Korn's inequality for nonconforming finite elements. *Technische Mechanik*, 20:205–214, 2000.

[6] Lacombe, F., Zapperi, S., and Herrmann, H. J. Dilatancy and friction in sheared granular media. *Eur. Phys. J. E*, 2:181–189, 1986.

[7] Nedderman, R. M. *Static and Kinematic of Granular Material*. Cambridge Uni. Press, Cambridge, New York, 1992.

[8] Ouazzi, A. *Finite Element Simulation of Nonlinear Fluids with Application to Granular Material and Powder*. Universität Dortmund, 2005. PhD thesis.

[9] Rannacher, R. and Turek, S. A Simple nonconforming quadrilateral Stokes element. *Numer. Methods Partial Differential Equations*, 8:97–111, 1992.

[10] Schaeffer, D. G. Instability in the evolution equation describing incompressible granular flow. *J. of Differential Equations*, 66:19–50, 1987.

[11] Schaeffer, D. G. *Mathematical Issues in the continuum formulation of slow granular flow*. Springer, 1997.

[12] Tardos, G. I. A Fluid Mechanics approach to slow frictional Powder Flows. *Powder Technology*, 15:61–74, 1997.

[13] Tardos, G. I., McNamara, S., and Talu, I. Slow and intermediate flow of a frictional bulk powder in the Couette geometry. *Powder Technology*, 4686:1–17, 2002.

[14] Turek, S. *Efficient solvers for incompressible flow problems: An algorithmic and computational approach*. Springer, 1999.

[15] Turek, S., Ouazzi, A., and Schmachtel, R. Multigrid Methods for Stabilized Nonconforming Finite Elements for Incompressible Flow involving the Deformation Tensor formulation. *J. Numer. Math.*, 10:235–248, 2002.